A Distributed Activation Energy Model of Thermodynamically Inhibited Nucleation and Growth Reactions and Its Application to the $\beta-\delta$ Phase Transition of HMX

Alan K. Burnham,* Randall K. Weese, and Brandon L. Weeks†

Lawrence Livermore National Laboratory, P. O. Box 808, Livermore, California 94551-0808

Received: April 17, 2004; In Final Form: September 16, 2004

Detailed and global models are presented for thermodynamically inhibited nucleation-growth reactions and applied to the $\beta-\delta$ phase transition of HMX (nitramine octahydro-1,3,5,7-tetranitro-1,3,5,7-tetrazocine). The detailed model contains separate kinetic parameters for the nucleation process, including an activation energy distribution resulting from a distribution of defect energies, and for movement of the resulting reaction interface within a single particle. A thermodynamic inhibition term is added to both processes so that the rates go to zero at the transition temperature. The global model adds the thermodynamic inhibition term to the extended Prout−Tompkins nucleation-growth formalism for single particles or powders. Model parameters are calibrated from differential scanning calorimetry data. The activation energy for nucleation (333 kJ/mol) is substantially higher than that for growth (29.3 kJ/mol). Use of a small activation energy distribution (∼400 J/mol) for the defects improves the fit to a powered sample for both the early and late stages of the transition. The effective overall activation energy for the global model (208.8 kJ/mol) is between that of nucleation and growth. Comparison of the two models with experiment indicates the thermodynamic inhibition term is more important than the energy distribution feature for this transition. On the basis of the applicability of the Prout−Tompkins kinetics approach to a wide range of organic and inorganic materials, both models should have equally broad applicability for thermodynamically constrained reactions.

1. Introduction

Although the basic concepts of gas- and liquid-phase kinetics and equilibria are part of standard undergraduate physical chemistry curricula, it is less widely appreciated that solid-state reactions are generally governed by nucleation-growth phenomena. Solid-state phase transitions are one type of solid-state reactions that are often governed by nucleation-growth reactions. The basic concept is that the reaction starts at a variety of nucleation sites, which grow in space via a reaction interface. The reaction spheres, or other shapes appropriate for the material, eventually coalesce and consume the entire material. The shape of the conversion-versus-time curve is sigmoidal. The two main lines of kinetic models for this process are the Prout−Tompkins[1] and Avrami−Erofeyev[2,3] approaches. While originally derived for solid-state reactions, they also have the correct mathematical form to model the thermal decomposition of many polymeric materials.[4,5]

The most common way to account for the temperature dependence of chemical and physical processes is with the Arrhenius equation, $k = A \exp(-E/RT)$. The activation energy, E, describes the amount of energy required to move from reactant to product, often over a barrier greater than the net energy change (enthalpy) of the reaction. One can usually relate the magnitude of the activation energy to a physical model in which the energy is comparable to that of the bonds involved and is most meaningful for an elementary reaction. For complex reactions, a global activation energy is often determined, which is a complicated average of the individual reaction steps. For free-radical propagation reactions in complex organic matter, for example, the global activation energy depends on a propagation-length weighted average of the initiation and propagation energies and is commonly one-half the initiation energy.[6,7]

Unfortunately, activation energies derived for chemical reactions can be higher or lower than the correct value due to the use of inappropriate kinetic models. Although the possible pitfalls are numerous, the one most pertinent to this paper is neglect of the effect of back-reaction, that is, thermodynamic inhibition, on the apparent activation energy. Vyazovkin mentions this problem in his recent review of solid-state kinetics.[8] An example particularly pertinent to this paper is the extremely high activation energies derived using Kissinger's method[9] to measure the kinetics of the $\beta-\delta$ crystallographic phase transition of nitramine octahydro-1,3,5,7-tetranitro-1,3,5,7-tetrazocine (HMX), which occurs at ∼175 °C with an enthalpy of 9.8 kJ/mol.[10] This transition involves a chair-to-boat conformational change, rearrangement of the crystalline lattice from monclinic to hexagonal, and a 6.7% volume increase.[11]

This problem of deriving the proper activation energy was addressed recently by Henson et al.,[12] who report a new kinetic model for the HMX phase transition. An important feature of their model is that the apparent activation energy approaches infinity near the thermodynamic transition temperature as the reaction rate approaches zero. Although this model is a significant advance over earlier treatments, it still has some limitations, which are described in more detail in following sections.

The objective of the current paper is to evaluate two alternate formalisms for thermodynamically inhibited nucleation-growth reactions. The first is a discrete-particle model, and the second is a phenomenological model in the spirit of Prout and

* To whom correspondence should be addressed. E-mail: burnham1@llnl.gov.

† Current address: Texas Tech University, Department of Chemical Engineering, Lubbock, Texas 79409-3121.

10.1021/jp0483167 CCC: $27.50
Published on Web 11/19/2004

Tompkins.[1] We measure kinetics for both individual particles and powdered samples, and we explore the relationships between the two models. Although relationship and utility of the models are demonstrated using the case example of the HMX, we consider the applicability and value of the models to be widespread over both inorganic and organic (including biological) materials.

The discrete-particle kinetic model assumes that nucleation occurs at crystal defects and that these defects have a distribution of energies. This defect energy distribution leads to a distribution of nucleation activation energies, which are equal to the activation energy of the defect-free material minus the defect energy distribution, which we describe with a Weibull distribution. Once nucleated, the growth velocity is governed by an Arrhenius rate constant. The time for an individual crystal to convert is determined by the time at which it initiates and the velocity of the transition wave. The time for an ensemble of crystallites to transform is given by an average over the defect and particle size distributions. Kinetic parameters are derived separately for the nucleation and growth processes of HMX. Although distributed activation energy models, including a Weibull model, are used commonly for fossil fuel chemical kinetics,[4] no comparable model appears to exist in the extensive literature for nucleation-growth reactions. The closest appears to be the heterogeneous stored-energy distribution model of Peczak and Luton[13] for dynamic recrystallization, in which the rate of nucleation is a function of the amount of stored energy in the vicinity of the nucleation site.

The phenomenological model is an extended Prout−Tompkins model having a thermodynamic inhibition term as introduced by Bradley[14] for solid-state reactions and included in the summary paper of Sestak and Berggren on nucleation-growth reactions.[15] This inhibition term is included in a recent Avrami-formalism model for nucleation and growth[16] and is commonly used for reactions such as carbonate decomposition.[17,18] Our version of this approach is used to fit HMX experimental data directly as well as synthetic data generated by the detailed nucleation-growth model, which was calibrated independently using HMX data.

2. Description of the Detailed Model

The chemical kinetic model to be solved is

$$\mathrm{A} \leftrightarrow \mathrm{B} \tag{1}$$

where two species A and B are able to interconvert. The transformation is governed by nucleation at a defect and growth across the particle. Nucleation is described as an activated process, and consequential nucleation can occur only when the phase transformation thermodynamics are favorable.

We can construct an effective forward rate constant of the form

$$k_{\mathrm{fn}} = A_{\mathrm{fn}} \mathrm{e}^{-(E_{\mathrm{fn}}-E_{\mathrm{d}})/RT} \tag{2}$$

where E_{fn} is the energy required to form a stable nucleus of phase B from a perfect crystal and E_{d} is the energy of a defect that could serve as nucleation site. R is the universal gas constant. Both A_{fn} and k have units of reciprocal time−volume. This is shown schematically in the top of Figure 1. It is also assumed that the nucleation process is first-order, although other orders are observed.[19] The probability that a crystal has nucleated is the time integral of the product of the rate constant, crystal volume, and time.

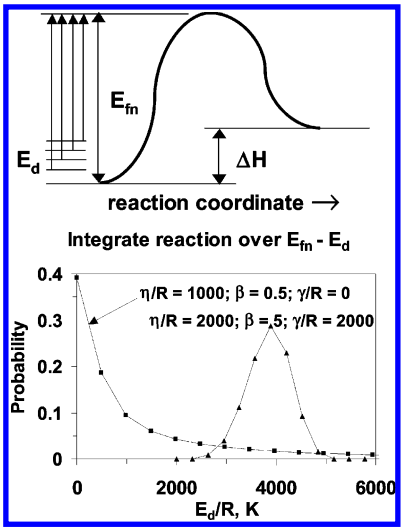

Figure 1. Schematic representation of the defect energy distribution kinetic model and two examples of defect energy distributions for representative Weibull parameters. β is dimensionless, and η/R and γ/R are in Kelvins. Each point represents a reaction channel in the Excel spreadsheet version of the detailed nucleation-growth model.

Phase B can also undergo reverse reaction characterized by the rate constant

$$k_{\mathrm{rn}} = A_{\mathrm{rn}} \mathrm{e}^{-E_{\mathrm{rn}}/RT} \tag{3}$$

where the subscript rn refers to reverse-nucleation. It is assumed here for simplicity that back-reaction creates a perfect starting material, although that need not be true in general. In the absence of defects, k_{fn} and k_{rn} are the relevant rate constants for defining the phase transition temperature. When $k_{\mathrm{fn}} > k_{\mathrm{rn}}$, phase B is the thermodynamically stable phase. When $k_{\mathrm{fn}} < k_{\mathrm{rn}}$, phase A is the thermodynamically stable phase. At $k_{\mathrm{fn}} = k_{\mathrm{rn}}$, the rate is zero. The equilibrium constant is $K_{\mathrm{eq}} = k_{\mathrm{fn}}/k_{\mathrm{rn}}$, so $K_{\mathrm{eq}} = 1$ at equilibrium.

If $k_{\mathrm{fn}} > k_{\mathrm{rn}}$, the reaction proceeds at some rate toward B with an effective rate constant k'_{fn} defined by

$$k'_{\mathrm{fn}} = k_{\mathrm{fn}}(1 - 1/K_{\mathrm{eq}}) \tag{4}$$

that is vanishingly small near equilibrium and gradually approaches k_{fn} as the distance from the equilibrium temperature increases. The concept of equilibrium concentrations, as in gas and solution reactions, is not relevant in this model, because the activities of the two phases are assumed to always be unity, and the reaction proceeds to completion for the most favored species. The effective reverse rate constant contains the same modifier.

There is a subtlety concerning the equilibrium constant that should be recognized explicitly. If defects are present, the question comes as to whether the local equilibrium constant should be between the defect state and the product or the perfect state and the product. In this model, we assume that the defect energies affect both the forward rate constant and local equilibrium constant; i.e., the back reaction remains constant, and we do not consider the case of annealing of defects.

Consequently, when E_{d} is nonzero, or more properly considered as having a distribution of values from 0 to some value considerably less than E_{fn}, the forward nucleation rate constant for nucleation is then given by

$$k'_{fn} = \int_0^\infty D(E_d) A_{fn} e^{-(E_{fn}-E_d)/RT}[1 - A_{rn}/A_{fn} e^{-(E_{rn}-E_{fn}-E_d)/RT}]\, dE_d \quad (5)$$

where $D(\ )$ is a distribution function, and the term in the brackets is the thermodynamic inhibition term in the presence of distribution of equilibrium coefficients due to the defect energy distribution. In practice, one determines the distribution of energy defects from the distribution of nucleation times for a variety of particles, or more precisely, from how that distribution varies from that expected from a first-order nucleation process.

For this model, $D(E_d)$ is assumed to follow a Weibull distribution,

$$D(E_d) = (\beta/\eta)[(E_d - \gamma)/\eta]^{\beta-1} \exp\{-[E_d - \gamma)/\eta]^\beta\} \quad (6)$$

where γ is the threshold energy, η is a width parameter, and β is a shape parameter. The Weibull distribution is used because it is mathematically flexible and can describe a variety of conceptually plausible distributions. The distribution is exponential in shape for small β and becomes more Gaussian as β increases. The mean activation energy is given by

$$E_{davg} = \gamma + \eta\Gamma(1/\beta + 1) \quad (7)$$

where $\Gamma(\ )$ is the gamma function. Two representative distributions are shown in the bottom portion of Figure 1.

The nuclei, once formed, rapidly expand by a growth process. The velocity of the reaction front is also assumed to follow an Arrhenius law,

$$k_{fg} = A_{fg} e^{-E_{fg}/RT} \quad (8)$$

where the subscript fg denotes forward growth. The rate constant for reverse growth, k_{rg}, has a corresponding definition. Both the forward and reverse growth constants have units of distance/time. Again, the propagation velocity is 0 at equilibrium, so one can write a net reaction rate

$$k'_{fg} = k_{fg}(1 - 1/K_{eq}) \quad (9)$$

Comparison of eqs 4 and 9 indicates

$$E_{fg} - E_{rg} = E_{fn} - E_{rn} \quad (10)$$

Here, we neglect the role of defects in the propagation velocity. Equation 10 is an outgrowth of assuming that the same equilibrium constant governs nucleation and growth.

HMX crystals are needlelike. Consequently, the interface initially expands more or less spherically until it reaches the sides of the crystal and then expands as a plane wave until it reaches the ends of the crystal, although not at an exactly uniform time. The nucleation site can occur at any point in the crystal. For any given crystallite, the conversion rate is a complicated function depending on the nucleation point and the crystal shape. Consequently, it can be considered most simply as a distribution of propagation distances. That makes the model general for any crystallite.

The distance traveled, s, in any direction is merely the product of velocity and time.

$$s = k_{fg} t \quad (11)$$

Consequently, the mean time required for the reaction interface to reach the edge of the crystallite is given by an average over the distribution of path lengths,

$$t = \int_0^{sp} D(s_i) s_i / k_{fg}\, ds_i \quad (12)$$

where $D(s_i)$ is distribution of those lengths from the nucleation site to the edge of a given particle, s_p is the maximum length for that particle, and

$$\int_0^{sp} D(s_i)\, ds_i = 1$$

The mass fraction reacted for any given path length, m_{xi}, is assumed to be linear,

$$m_{xi}(t) = s/s_i \quad (13)$$

where s_i is the maximum distance in the ith direction, so s/s_i is constrained to ≤ 1. The total mass fraction converted over the entire crystallite is given by average over the distribution of path lengths:

$$m_x(t) = \int_0^{sp} D(s_i) s/s_i\, ds_i = \int_0^{sp} D(s_i) k_{fg} t/s_i\, ds_i \quad (14)$$

We assume that all path lengths are equally probable.

The model was implemented in an Excel spreadsheet using simple explicit numerical integration. The defect energy distribution was represented by 16 discrete reaction channels and used to generate a nucleated fraction versus time. Each of these reaction channels was subdivided into six components, which correspond to the initial and final 10% nucleated and four intermediate nucleation probability intervals of 20% each. The growth of each of these nucleated components, in turn, was averaged over 20 evenly spaced growth distances. The model calculations contain some graininess due to the finite number of channels, but not as much as data for milligram-sized samples.

In an ensemble, of course, the mass conversion must be averaged over the distribution of s_p (i.e., particle size distribution). One might expect that larger particles would take longer to react than smaller particles, but that is not necessarily the case. The probability of nucleation increases with size, and the reaction time is a competition between the rate of nucleation and the rate of growth. If the growth time is smaller than the time between nucleation events, the large particles will convert sooner. This is somewhat analogous to the fact that composites of small defect-free fibers can be stronger than large defect-rich fibers.

We observed the reaction growth interface traversing crystal boundaries in our optical studies. Consequently, a large particle assembly could react faster than predicted from the distribution of individual crystallites. In principle, the model could incorporate a resistance function for cross-boundary growth, but that is beyond the scope of the present work. One might expect this resistance factor to depend on the type of contact between the crystallites.

3. Description of the Global Kinetic Model

While more explicit physically, the detailed model is difficult to calibrate routinely because of the nine reaction parameters needed for ensembles of individual particles. Furthermore, there is no simple way of treating the intergrain propagation. Consequently, we adopted a simpler phenomenological model for thermodynamically inhibited nucleation-growth reactions derived by simply adding the thermodynamic constraint factor to an extended Prout−Tompkins model,

$$dx/dt = -kx^n(1 - qx)^m(1 - 1/K_{eq}) \quad (15)$$

where x is the fraction remaining, n is a reaction order, m is more correctly defined as a nucleation-growth parameter, and q is an initiation parameter. When far from equilibrium and when $m = 0$ and $n = 1$, this reduces to a first-order reaction. The conventional Prout−Tompkins model has $n = m = 1$. The conventional Prout−Tompkins model can be integrated analytically only for constant temperature. The parameter q is related to the initial condition (integration constant) that enables the reaction to get started, since dx/dt is identically 0 at $x = 1$ for the Prout−Tompkins model as normally written. Equation 15 is included in the most recent version of Lawrence Livermore National Laboratory (LLNL) kinetics analysis program (Kinetics05).[4] Equation 15 is numerically integrated over the relevant experimental conditions, typically (but not restricted to) isothermal and constant heating, and multiple data sets are fitted simultaneously by nonlinear regression. An analogous equation could be written for the Avrami−Erofeyev approach by replacing $(1 - qx)^m$ by $(-\ln (qx)^p)$, where p is the growth dimensionality in the Avrami formalism.[15]

Now consider that eq 15 is not reversible for solid-state reactions in the way it would be for homogeneous reactions. One could write a net reaction rate having nucleation-growth rate laws in both directions.

$$\mathrm{d}x/\mathrm{d}t = -k_f x^n (1 - x)^m - k_r (1 - x)^n x^m \qquad (16)$$

In this case, x indicates a mass fraction of component A, so the exponents are switched in the forward and reverse terms. For simplicity, the q factor is not shown explicitly. Note that in the limit of $n = m$, one can factor out the k's to form an equation equivalent to eq 15, since $K_{eq} = k_f/k_r$. However, the physical rationale for the form of the Prout−Tompkins model is not valid for complete reversibility along the reaction coordinate.

As pointed out by Avrami[2] more than 60 years ago, expanding growth regions consume unnucleated defects and eventually coalesce with neighboring growth regions. While the reaction interface could be reversed over some infinitesimal distance, it can neither retrace its steps once coalescence has occurred nor reconstruct the original defect distribution. Consequently, we consider eq 15 to be unidirectional. Once the reaction is complete, one could use the same equation in the reverse direction, albeit with a different defect energy distribution characteristic of the product material, but eq 15 is not a valid way to treat extensive reversibility during the course of the reaction.

Equations 15 and 16 have both similarities and differences from that of Henson et al.[12] They construct a kinetic equation with both forward and reverse first-order reactions more along the lines of eq 16. Their additional first-order term relates more explicitly to nucleation than the traditional Prout−Tompkins model, which we modify in a different manner. We previously showed[20] that the first-order term in the nucleation-growth formalism of Nam and Seferis[21] is equivalent to our q factor if the activation energies are the same for the first- and second-order processes. In addition, a nucleation-growth reaction is not reversible to any substantial extent along the same reaction pathway, as stated earlier. Consequently, we consider eq 15 a better approach for incorporating thermodynamic inhibition phenomenologically than either eq 16 or the equations of Henson et al.[12]

4. Experimental Methods

A. Samples. Three sources of pure β-HMX were used in this study. One material (batch B-844) was manufactured by Holston Defense Corporation (HOL 81H030-033) for LLNL using the Bachmann synthesis process and was determined to be >99.90% pure as analyzed by HPLC for RDX impurities. Particle-size analysis indicated that >90% of the material was between 30 and 500 μm in diameter. Other DSC experiments used crystal fragments derived from a large single crystal of β-HMX grown by H. H. Cady and provided to LLNL by the University of Delaware. Fragments averaging 1-mm diameter were used. A few experiments used the HMX formulation PBX 9501, a blend of 95% HMX, 2.5% Estane, and 2.5% BDNPA-F. For the optical studies, pure β-HMX crystals were prepared by the method of Siele et al.[22] Octahydro-1,5-diacetyl-3,7-dinitro-1,3,5,7-tetrazocine (DADN) was treated with 100% HNO_3 and P_2O_5 at 50°C for 50 min, followed by quenching in ice water. Slow recrystallization from acetone yielded HMX as colorless microcrystals.

B. Reaction Measurements. Optical movies were recorded to help understand earlier AFM experiments.[11] A Leica optical microscope (total magnification 800×) was used for the dynamic movies to determine the velocity of the phase transition within individual crystals. The size of each crystal was determined with a calibrated reticle. Movies were recorded in real time using a color CCD camera and a standard VCR. Sample heating was accomplished using a Veeco temperature controller. The samples were heated from ambient temperature to 300 °C with a ramp rate of 20 °C/min. The resolution of the heater stage is 0.2 °C, and the small size of both the sample and the heating stage ensures uniform heating over the entire crystal. Movies are available as Supporting Information.

A differential scanning calorimeter (DSC), TA Instrument model 2920, and its associated software, Universal Analysis, were used for additional analyses. All data were collected at 0.2 s^{-1}. DSC[23] measures the difference in the heat flow between a sample and an inert reference as a function of time, where both the sample and the reference are subjected to a controlled temperature−pressure environment during that time. The instrument design used here is commonly called the heat flux design. Indium, tin, lead, and zinc from TA Instruments were used to calibrate the temperature and enthalpy response of the instrument at a heating rate of 10 °C/min. Onset temperatures at other heating rates were corrected using measurements of indium and tin melting points at 0.5, 5, 25, and 100 °C/min.

All samples were weighed in a Sartorius MC 5 Electronic balance accurate to ≤0.005 mg. In all cases, the pan with sample was matched to a reference pan within 100 μg to balance heat flows due to heat capacity.

5. Calibration of the Detailed Model for HMX. The nucleation and growth aspects of the detailed model are calibrated separately. We start with general observations, followed by a calibration of the growth kinetic parameters, because they are simpler to extract. Nucleation kinetic parameters, which are more difficult to extract, are then estimated.

The reaction rate of the phase transition is assumed to be proportional to heat flow. Representative calorimetry traces are shown in Figure 2 for 0.4-mg samples of HMX batch B-844. At slow heating rates for small samples, one can discern individual particles undergoing the phase transition. At higher heating rates, the individual grain resolution is lost, because the lower activation energy for growth than for nucleation makes the individual peaks broader in temperature. The distribution of nucleation times reflects the probabilistic nature of nucleation. The envelope outlined by many crystals reflects both the basic rate law (e.g., first-order) for the nucleation process and any distribution effects related to particle size, defect energy, or both.

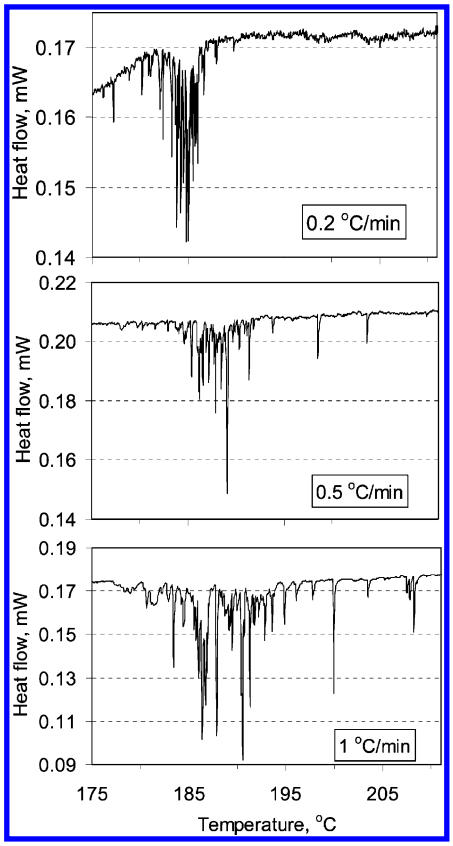

Figure 2. Heat flow thermograms from a differential scanning calorimeter for 0.19−0.37-mg samples of HMX batch B-844. The individual spikes are from conversion of individual grains. The integrated endotherms for 12 samples averaged 9.6 kJ/mol (σ = 0.7 kJ/mol, and no dependence on heating rate over 0.1 to 1.0 °C/min), which is well within literature values.

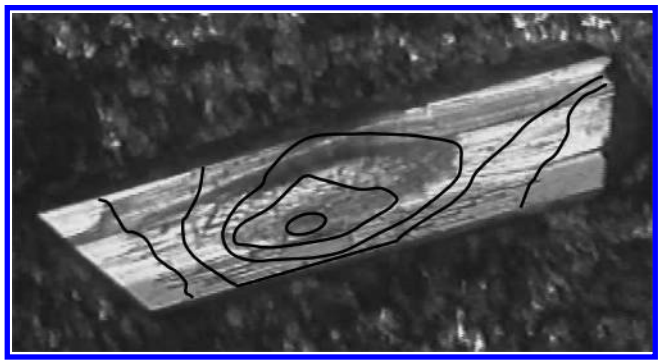

Figure 3. Optical micrograph of 250-μm × 60-μm monoclinic HMX crystal. The phase transition started at ∼178 °C. The black contour lines represent an estimate of the reaction interface at 1, 4, 7, 12, and 16 s after nucleation. The total conversion took ∼20 s, with a maximum propagation distance of ∼140 μm.

A. Growth Kinetic Parameters. Optical movies show that the transformation clearly starts at a specific site, then propagates across the crystal. Two shades of textural changes are visible, which was also observed by AFM,[11] but they occur close enough in time that the difference does not materially affect the average growth velocity. Approximate contours of the reaction interface as a function of time are given for one crystal in Figure 3. Although the reaction interface does not propagate smoothly, one can estimate an approximate average reaction velocity for this particle of ∼7 μm/s at 178 °C. Movies of a second crystal yielded an average velocity of 19 μm/s at 182 °C. Other movies, for which the initial temperature is not well specified, show phenomena such as multiple initiation sites at different times and initiation of the transition in one crystal upon contact with the reaction front from an adjacent crystal.

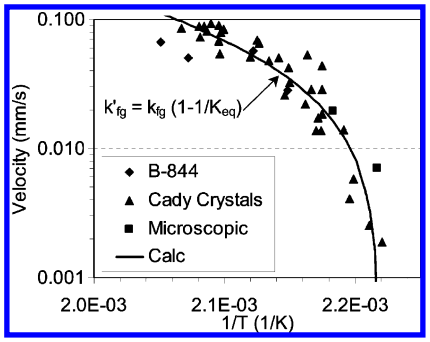

Figure 4. Summary of growth velocity measurements on HMX and a fit to the thermodynamically inhibited growth model embodied in eq 9, yielding $k_{fg} = 850 \exp(-3523/T)$.

To get enough velocity−temperature points to properly determine kinetic parameters, endotherms of individual particles with an average diameter of 1 mm were measured by DSC. Average velocities were estimated from the width of the endotherm (baseline-to-baseline within a few percent) and the particle mass, as measured by simultaneous thermogravimetric and differential thermal analysis. An HMX density of 1.9 g/cm^3 was used. Since the particles are enlongated, the average propagation was assumed to be 1.5 times the effective spherical diameter.

The velocities from both measurement methods are plotted versus $1/T$ in Figure 4 for two sources of crystals. The points fit well to eq 9, which predicts that the velocity should go to zero at the transition equilibrium temperature. Values for the equilibrium constant were derived from Henson et al.,[12] who report a transition enthalpy of 9.8 kJ/mol (2.35 kcal/mol) and show a measured phase transition temperature at atmospheric pressure of ∼451 K (178 °C) in their Figure 4. A dimensionless preexponential factor of 13.8 results in a calculated phase transition temperature of 177.5 °C.

A corollary prediction of the interfacial velocity going to zero is that the apparent activation energy for growth approaches infinity near the transition temperature. Analyzing the data above and below 192 °C separately yields apparent activation energies of 300 and 60 kJ/mol, respectively, far from and near to the transition temperature. In contrast, taking the thermodynamic inhibition explicitly into account, one derives an uninhibited, forward Arrhenius function for $\beta \rightarrow \delta$ interfacial growth.

$$k_{fg} = 850 \exp(-3523/T) \text{ mm/s} \qquad (17)$$

The forward activation energy of 29.3 kJ/mol is three times that of the phase transition enthalpy and 42% of the melting enthalpy. The high-temperature limit of the transition velocity is nearly 1 m/s, which is substantially lower than the room-temperature sound velocity.

B. Nucleation Kinetic Parameters. Given enough individual particle measurements, the curves defined by the cumulative fraction of nucleated particles at different heating rates as in Figure 2 could be used to directly determine Arrhenius parameters for nucleation. However, powder experiments suffer from reaction-profile overlap and the possibility of cross-particle nucleation. Single particle experiments are too time-consuming to gather completely satisfactory statistics. Consequently, the nucleation parameters cannot be determined as accurately as the growth parameters.

Nevertheless, we can explore general limits to the parameters by overlaying the predicted beginning and end of nucleation

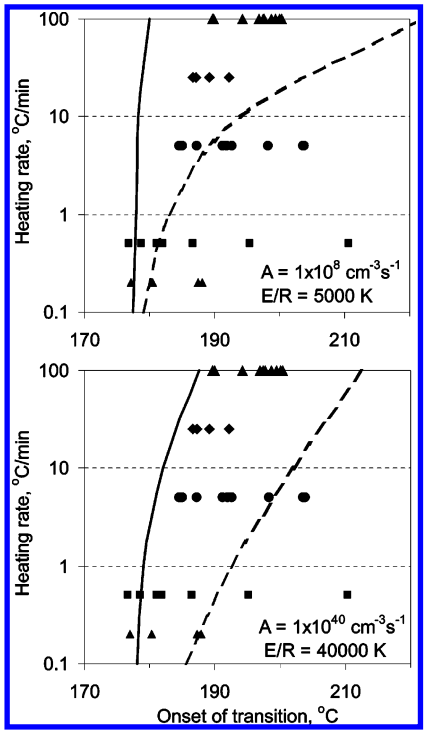

Figure 5. Example of the inability of a first-order nucleation model with low (top) and high (bottom) activation energies to fit the distribution of transition onset temperatures for Cady crystals. A different symbol is used for each heating rate. The solid line represents a 1% nucleation probability, and the dashed line represents a 99% nucleation probability, using eq 4 and a particle size of 1 mm.

(1% and 99% points calculated using eq 4) with the measured onsets for several single particles at each of five heating rates (Figure 5). The onset is the first point in the endotherm that noticeably deviates from the baseline and has an uncertainty ranging from ~0.1 to 1 °C as heating rate increases from 0.1 to 100 °C/min. The calculations used a particle diameter of 1 mm—the same as in the experiments. Comparison of measured and calculated nucleation events is given in Figure 5. The quality of agreement is judged by how closely the onset events are bounded by the two curves.

The top of Figure 5 shows a comparison using a low activation energy comparable to that obtained for interfacial growth. The agreement is not good. It is not difficult to fit the leading edge of the nucleation events (solid line) with a low activation energy—there are an infinite number of A−E pairs defined by a typical compensation law. The problem is that the completion of nucleation (dashed line) is missed at high heating rates for a low activation energy, which requires that nucleation occur over a very narrow interval at low heating rates and a wide interval at high heating rates. Decreasing the frequency factor to 3×10^6 cm^{-3} s^{-1} shifts the 1% nucleation point at 100 °C/min to 191 °C, but it also shifts the 99% nucleation point to 325 °C, which is 100 °C too high. Adding a distribution of energies to a low average defect energy does not solve the problem. The effect of a distribution is to shift the whole curve at any particular nucleation fraction to higher temperature. The fit improves at low heating rates but becomes worse at high heating rates.

After considerable searching, we concluded that only a very high activation energy, >300 kJ/mol, provides a reasonable fit to the data. Such a fit is shown in the bottom of Figure 5. The data are explained to within the statistical uncertainty of limited nucleation events. No energy defect distribution is apparent at this level of precision. The challenge now becomes

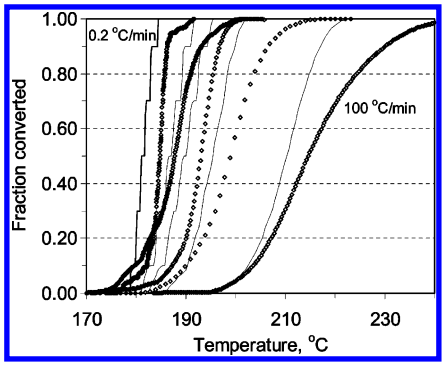

Figure 6. Comparison of the detailed model (lines) calibrated on a small number of Cady crystals to experimental data (points) for HMX batch B-844. The point/line pairs vary from 0.2 °C/min on the left to 100 °C on the right. The steps observed in the low heating rates are due to the use of only six nucleation fractions. At high heating rates, growth is slow compared to nucleation, so these steps are blurred.

to explain the physical interpretation of such a high average energy. As noted previously by Henson et al.,[12] this is difficult to understand physically, and they interpret it as a reflection of the ratio of molecules in the active state.

An alternative explanation is that the high activation energy reflects the cooperative motion of several molecules, so the energy per chemical bond is still relatively small. A similar effect is observed for denaturation of proteins, which requires the breaking of many hydrogen bonds along a chain. Effective activation energies are sometimes very high,[24] giving rise to the concept of an effective cooperative unit. A definitive explanation of the value of the nucleation activation energy is a matter for future exploration.

6. Comparison of Detailed and Global Models for HMX. The detailed model can be compared both directly and indirectly to experimental data for HMX. Figure 6 shows a comparison of the measured fraction converted for batch B-844 versus that calculated by the detailed model. The detailed model was calibrated against certain reaction characteristics of a limited number of Cady crystal fragments (Figure 5 bottom), not a fit to the reaction profile of a statistically large sample, so the qualitative agreement is confirmation of the validity of the general approach.

Limitations of the data-model concurrence are more pronounced at low heating rates, in part due to the granularity related to the assumption of six nucleation fractions for the interfacial propagation calculations. In addition, low and high temperature tails on the B-844 reaction profiles may reflect the presence of a distribution of defect energies not evident in the calibration against a limited number of nucleation events. As a result, Figure 7 compares the nucleated fractions directly with the fraction converted, both with and without a small detect energy distribution (η = 418 J/mol). To maintain the 50% conversion point at roughly the same temperature, the defect distribution was shifted by its mean (375 J/mol) so that it is roughly symmetrical about zero. An additional factor at the highest heating rates might be thermal gradients within the particles, which would broaden the profile.

Although the detailed model is able to simulate the conversion over wide range of thermal conditions, it is more complicated than desirable for routine application. Consequently, we explored the ability of the thermodynamically inhibited Prout−Tompkins formalism to correlate both synthetic data from the detailed model and the experimental data for batch B-844. The results for these two fits are shown in Figure 8. The global kinetic parameters are summarized in Table 1. The parameters are very

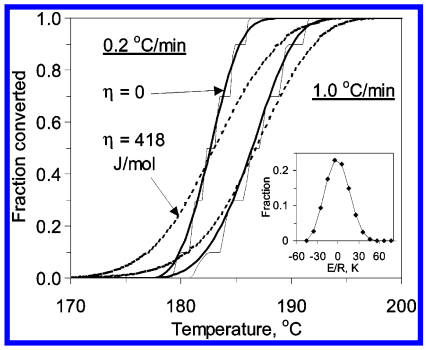

Figure 7. Comparison of the binned nucleation-growth model with detailed nucleated fraction calculations with and without a defect energy distribution, η. The mean of the defect distribution (insert) is adjusted to 0 so that the 50% nucleation point is nearly constant, and $\beta = 3$. The dashed line represents the use of the same distribution at both heating rates. The effects of a distribution on the early and late conversion is qualitatively similar to that observed for batch B-844 (Figure 5).

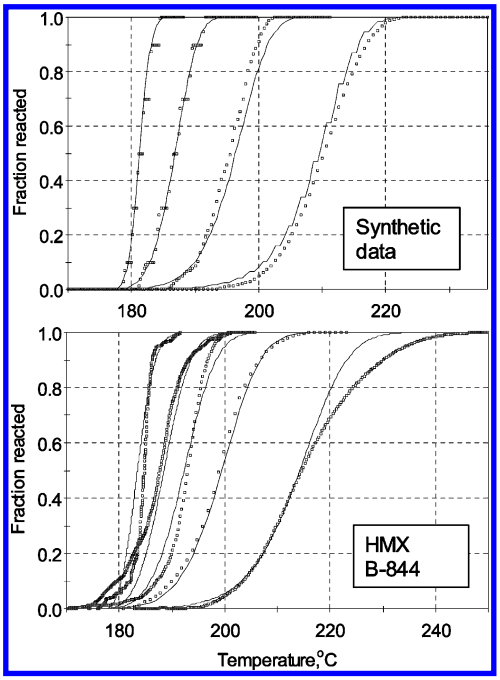

Figure 8. Fit of synthetic from the detailed nucleation-growth model (top) and experimental data for HMX batch B-844 (bottom) to the global thermodynamically inhibited nucleation-growth model, eq 15. The synthetic data was calculated at 0.1, 1.0, 10, and 100 °C/min, and experimental data is at 0.2, 1.0, 2.5, 10, and 100 °C/min. The resulting kinetic parameters are given in Table 1.

TABLE 1: Effective Kinetic Parameters Determined from Synthetic and Real Data for the Thermodynamically Inhibited, Extended Prout−Tompkins Model

data type	method	A, s^{-1}	E/R, K	nucleation parameter, m	reaction order, n
synthetic data[a]	$T_{50\%}$-shift	1.71×10^{44}	49 722		
	NLR	1.80×10^{25}	27 777	0.299	1.00
HMX B-844	$T_{50\%}$-shift	3.92×10^{37}	42 845		
	NLR	2.91×10^{22}	25 116	0.180	1.17

[a] Created using $k_{fn} = 5.23 \times 10^{36} \exp(-40000/T)(1 - 1/K_{eq})$ s^{-1}; $k'_{fg} = 850 \exp(-3523/T)(1 - 1/K_{eq})$ mm/s; $K_{eq} = 13.8 \exp(-2350/T)$.

similar for the synthetic and real data. A reaction order of greater than one is mathematically equivalent to a gamma distribution of frequency factors,[4] which may reflect a distribution in either particle sizes or defect energies. The apparent activation energy

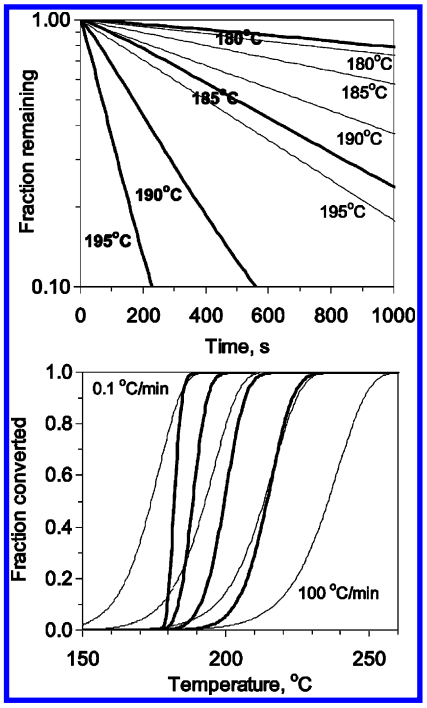

Figure 9. Comparison of calculated fractions reacted from the kinetic expressions of Brill and Karpowicz[25,26] (thin lines) and the nonlinear regression parameters for sample B-844 from Table 1 (bold lines). The top figure is for isothermal conditions, and the bottom is for heating rates of 0.1, 1.0, 10, and 100 °C/min. The Brill−Karpowicz kinetic model does not agree well with our data over wide temperature ranges.

from the nonlinear regression analysis is between those for nucleation and growth. The higher activation energy from the shift in the 50% conversion temperature is equivalent to using Kissinger's T_{max} method and demonstrates the pitfall of using that method near a thermodynamic transition. The energies from the $T_{50\%}$ method are similar to those reported earlier by Weese et al.[10]

7. Comparison to Other Kinetic Models. One of the most widely recognized kinetic models for the $\beta \rightarrow \delta$ HMX phase transition is the work of Brill and Karpowicz.[25,26] They report from isothermal experiment using infrared spectral changes that the reaction is first-order in the temperature range of 171−185 °C, with $E = 204$ kJ/mol and $A = 1 \times 10^{20}$ s^{-1} (actually, $10^{19.9}$ in ref 25 and $10^{10.1}$ in ref 26). An obvious discrepancy is that our pure HMX does not decompose below 175 °C. We do find the transition to occur at lower temperature in HMX formulations with a binder, such as PBX 9501, which transforms at 170 °C. Single-particle onset temperatures for PBX 9501 have a similar pattern as in Figure 5 but are shifted ~5 °C lower than the Cady crystal fragments.

We do not find the overall reaction to be first-order, so our model parameters cannot be compared directly to Brill's work. Instead, we compare conversion curves for both isothermal and constant heating rate conditions in Figure 9. The conversions are very similar at 180 °C, but our expression becomes much faster at higher temperature. Because the reaction is only weakly autocatalytic, the curvature in the Arrhenius plot is not particularly visible for the small conversion ranges measured by Brill et al., so their report that the reaction is first-order is not definitive. At a constant heating rate, their expression calculates the transition in the right temperature region, but it does not agree well quantitatively with either our data or our model. The disagreement at slow heating rates, of course, is due to a lack of a thermodynamic constraint for their kinetic

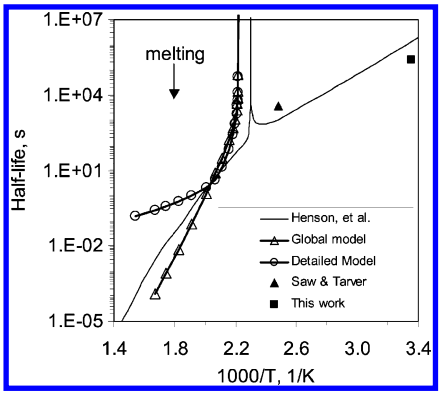

Figure 10. Comparison of the kinetic models of Henson et al.[12] and from this work. All predict that the half-life and activation energy go to infinity close to the transition temperature. The 10 °C difference in transition temperatures can be ascribed largely to the differences in sample. The curvature of the detailed model is due to the assumption of a single nucleation site per grain, which is not universally valid. Our models do not claim quantitative knowledge of the reversion portion of the curve, because the defects and grain sizes governing the reversion kinetics differ from the starting material. All the models predict the transition to be rapid compared to the time to explosion.

model, but their expression also predicts the transition to shift to much higher temperatures under rapid heating than we observe.

Henson et al.[27] derived phase transition kinetics, as measured by second harmonic generation (SHG) during slow heating, for a second-order kinetic model equivalent to a Prout−Tompkins model. They obtained an A and E similar to Brill's group, although a quantitative comparison would require plotting the two functions, as in Figure 9. Our activation energy and frequency factor from the modified Prout−Tompkins approach are similar, although slightly higher. However, Henson's first model is not thermodynamically constrained, and we calculate that the phase transition would be complete in ∼40 min at 160 °C, which is far below the phase transition.

Both our detailed and global models are similar to the second model of Henson et al.[12] in that a thermodynamic constraint requires the reaction rate to approach zero and the apparent activation energy to approach infinity as the reaction approaches the phase transition temperature. A comparison of calculated half-lives for our two models and their model is shown in Figure 10. Our global model agrees qualitatively with Henson's model. The 10 °C difference in transition temperature is probably due to differences between their PBX 9501 formulation and our purer forms.

Between the transition temperature and ∼215 °C, our global model essentially overlays the detailed model calculation for 1-mm particles, but at higher temperatures, the two half-lives diverge as the growth activation energy dominates the conversion curve in the detailed model. Our detailed model assumes only one nucleation site per crystal, which would be true only for nearly perfect crystals. Consequently, the detailed model calculates that smaller particles last longer in the nucleation-dominated range below 250 °C and last a shorter length of time in the growth-dominated regime at higher temperatures. The true dependence on particle size is beyond the scope of our data, but this result points out the importance of knowing whether the number of nucleation sites is proportional to volume, to particles, or something in between. However, the issue becomes unimportant above the melting point of ∼280 °C.

Smilowitz et al.,[28] in a companion paper to Henson et al.,[12] report conversion and reversion kinetics by SHG for individual HMX crystals and HMX formulation PBX 9501. For individual

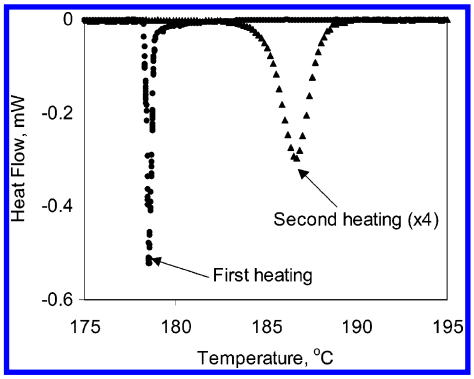

Figure 11. Comparison of first and second cycle $\beta \rightarrow \delta$ phase transitions for a single fragment of the Cady crystal. Both the shift in T_{max} and broadening of the profile reflect differences in the defect and porosity structures of the material. This is a basic proof that nucleation-growth kinetics cannot be considered to be reversible in the homogeneous reaction sense.

crystals, they note that the nucleation time is variable and attribute this variation to different nucleation energies, which would be treatable with our distributed energy model. Unfortunately, the nucleation time for a single crystal nucleation event is a probabilistic quantity, so it is not quite that simple. Just as in our Figure 5, insufficient numbers of onset times were reported to separate small energy distribution effects from the underlying nucleation kinetic law. In addition, they report reversion kinetics that generally follow their calculated half-life curve, but they do not get a good universal fit for all experimental conditions.

Saw[29] and Saw and Tarver[30] monitored the conversion and reversion of both neat HMX and PBX 9501 by X-ray diffraction (XRD). They observed negligible reversion after 4 h at room temperature for neat HMX, but reversion starts at ∼130 °C during cooling for PBX 9501 in similar experiments. They concluded that reversion is influenced by the polymer binder. Upon repeated cycling, they also observed that each successive reversion required a longer time. They also report that complete reversion takes longer than 2 h at 130 °C, and their data suggest a half-life of ∼1 h. That point is plotted on Figure 10 and is qualitatively similar to the SHG measurements reported by Smilowitz.[28]

Although we did not conduct extensive experiments to characterize the reversion kinetics, we conducted a few experiments in which a sample was converted, cooled at various conditions, and then heated again to measure the amount reverted. Figure 11 shows a typical result of one such experiment using a single crystal, in which the sample was heated at 0.5 °C/min to 198 °C, cooled naturally over an hour to room temperature, and maintained there for 5 days prior to being heated again at 0.5 °C/min to 200 °C. The sharp peak for the first heating is consistent with Figure 2 in that Figure 2 is a collection of such sharp spikes from a group of small crystals. The transition profile for the second heating is both at a higher temperature and substantially broader than for the initial transition. This reflects the differences in defects and porosity in the resulting polycrystalline material after conversion/reversion. That the conversion kinetics change after conversion/reversion confirms that the reaction cannot be considered reversible in a simplistic sense.

Nevertheless, we can estimate a rate constant from the observation that no substantial reversion is detected upon such second heating for times less than 10 h and that the transition enthalpy after the 5-day room temperature exposure corresponds to 72% of the original value. This implies an approximate value

of the half-life of 3 days at room temperature, which is plotted in Figure 10 and is qualitatively consistent with the model of Henson et al.[12] It is also qualitatively consistent with the first observations of Saw.[29] Note, however, that this point is on the opposite side of the line from Saw and Tarver, so there are quantitative discrepancies.

Zaug et al.[31] report simultaneous measurements of the conversion and reversion using SHG and XRD and find that the SHG measurements do not overlap with XRD measurements near the transition temperature. At a constant temperature of 165 °C, SHG followed a first-order increase ($1 - e^{-kt}$), whereas the XRD followed a sigmoidal curve (implying nucleation growth) that lagged the SHG result by about 10^4 s. They suggest that the SHG measurement is strongly influenced by surface roughening[11] and does not represent a bulk conversion. A quantitative comparison to our kinetic model is complicated by the fact that our model is calibrated on material that did not convert to the δ phase below 175 °C. However, Zaug's results indicate one must be cautious comparing quantitatively the SHG results reported by Smilowitz et al.[28] and the models either in this work or of Henson et al.[12] Consequently, we conclude that there are still unresolved issues about the quantitative correspondence of phase transition kinetics measured by different techniques that are beyond the scope of this paper.

8. Summary

The $\beta \rightarrow \delta$ crystallographic transition of HMX clearly follows a nucleation-growth mechanism, as can be seen clearly from optical micrographs. Consequently, one can construct a detailed conversion model in which the nucleation and growth processes are treated separately and explicitly. Although the conversion is not reversible along the same reaction pathway to a material with the same physical properties, a thermodynamic inhibition term can be added to both the nucleation and growth kinetic terms that cause the reaction to slow near equilibrium and stop at equilibrium.

The phase transition tends to start at visible defects, which suggests that the nucleation activation energy is decreased from its value for a perfect crystal by the defect energy. A nucleation model has been constructed in which the defect energies can be parametrized by a Weibull distribution, which can vary from near exponential to near Gaussian, with any chosen width and threshold energy.

Especially at low heating rates, the DSC thermograms consist of a series of sharp spikes, which usually represent the transition of individual crystals, although optical movies show that the transition of a given particle can sometimes initiate the transition of a contacting particle. The velocity of the reaction front can be observed directly, and the velocity measured in this way agrees with that calculated from the width of the transition of an individual particle and its mass, hence size.

The interfacial velocity has been measured on single particles by both techniques. When plotted on an Arrhenius diagram, the velocities form a curve that heads toward zero at the transition temperature, which validates the model of an Arrhenius velocity modified by a thermodynamic inhibition term. The apparent activation energy derived from the instantaneous slope varies from ~60 kJ/mol tens of degrees from the transition to hundreds of kJ/mol near the transition. This agrees conceptually with an earlier model of Henson et al.[12] for the transition as a whole. Removing the thermodynamic inhibition contribution results in uninhibited activation energy for interfacial growth of ~30 kJ/mol, which is three times the transition enthalpy and 42% of the melting enthalpy.

The nucleation kinetics can be derived from the distribution of onset temperatures for individual crystals. Although the number of onset temperatures measured is not sufficient to precisely determine the Arrhenius parameters for nucleation, an apparent activation energy in excess of 300 kJ/mol appears likely, even after removing the thermodynamic inhibition term. The physical interpretation of this activation energy, which is higher than the enthalpy of sublimation, is unclear. It may reflect the need for a cooperative reaction among several molecules to get the transition going.

When combined, the separately calibrated nucleation and growth kinetics agree with the observed rate of phase transition measured by DSC at heating rates from 0.2 to 100 °C/min. Because of the low activation energy for growth, the profile widths for individual crystals become larger than the spacing between nucleation events, and the reaction profile of an assembly of particles becomes fairly smooth at high heating rates. As particle size increases, the difference between the fraction nucleated and fraction converted becomes substantial for particle sizes on the order of 1 mm at temperatures >200 °C.

Although the detailed model has the capability to calculate effects of particle size on transition kinetics, one must realize that an implicit assumption of the current model is that the nucleation site (defect) density is constant per unit volume. This means that smaller particles are less likely to initiate, and when they do, less volume is consumed. Of course, it is equally probable that, depending on how the material is prepared, particles of all sizes have the same number of defects. Prediction of particle-size dependence is outside the scope of the current calibration.

While the detailed model is conceptually attractive, it is cumbersome for routine engineering use. Consequently, a phenomenological model has been created by adding the thermodynamic inhibition term to an extended Prout−Tompkins model. This model fits the data well over a wide range of heating conditions, and the apparent activation energy is midway between those of nucleation and growth. Unfortunately, if one looks at even larger temperature intervals, the phenomenological model is not able to track any change in effective activation energy over the transition from nucleation-dominated kinetics to growth-dominated kinetics.

The concepts of nucleation and growth permeate a wide range of fields. The sigmoidal mathematical form of the Prout−Tompkins model gives it the ability to fit the formation of final product in a sequential reaction.[32] It has the ability to fit reaction profiles ranging from linear polymer decomposition to mineral dehydration to the release of implanted gas from solid surfaces.[20] Adding a thermodynamic inhibition term should enable it to model the phase transformations in a broad range of organic and inorganic materials over modest temperature intervals near the phase transition.

Acknowledgment. We thank those who assisted parts of this work, including Robert Braun, who added the thermodynamically inhibited model to the Kinetics05 code, Kevin Vandersall and Frank Garcia for supplying the high explosive material, Mark Hoffman for sample characterization, and Heidi Turner for running some of the DSC experiments. This work was performed under the auspices of the University of California Lawrence Livermore National Laboratory under contract number W-7405-Eng-48.

United States Government nor the University of California nor any of their employees, makes any warranty, express or implied, or assumes any legal liability or responsibility for the accuracy, completeness, or usefulness of any information, apparatus, product, or process disclosed, or represents that its use would not infringe privately owned rights. Reference herein to any specific commercial product, process, or service by trade name, trademark, manufacturer, or otherwise does not necessarily constitute or imply its endorsement, recommendation, or favoring by the United States Government or the University of California. The views and opinions of authors expressed herein do not necessarily state or reflect those of the United States Government or the University of California, and shall not be used for advertising or product endorsement purposes.

Supporting Information Available: Movies discussed in the Reaction Measurements section are available as Supporting Information. This material is available free of charge via the Internet at http://pubs.acs.org.

References and Notes

(1) Prout, E. G.; F. C. Tompkins, *Trans. Faraday Soc.* **1944**, *40*, 488.
(2) Avrami, M. J. *J. Chem. Phys*. **1939**, *7*, 1103; **1940**, *8*, 212; **1941**, *9*, 177.
(3) Erofeev, B. V. *C. R. Dokl. Akad. Sci. USSR* **1946**, *52*, 511.
(4) Burnham, A. K.; Braun, R. L. *Energy Fuels* **1999**, *13*, 1.
(5) McCoy, B. J. *Ind. Eng. Chem. Res*. **1999**, *38*, 4531.
(6) Jellinek, H. H. G. In *Aspects of Degradation and Stabilization of Polymers*; Jellinek, H. H. G., Ed.; Elsevier: Amsterdam, 1978; p 26.
(7) Weres, O. *Org. Geochem*. **1988**, *12*, 433.
(8) Vyazovkin, S. *Int. Rev. Phys. Chem.* **2000**, *19*, 45.
(9) Kissinger, H. E. *J. Res. Natl. Bur. Stand.* **1956**, *57*, 217.
(10) Weese, R. K.; Maienschein, J. L.; Perrino, C. T. *Thermochim. Acta* **2003**, *401*, 1.
(11) Weeks, B. L.; Ruddle, C. M.; Zaug, J. M.; D. J. Cook, *Ultramicroscopy* **2002**, *93*, 19.
(12) Henson, B. F.; Smilowitz, L.; Asay B. W.; Dickson, P. M. *J. Chem. Phys*. **2002**, *117*, 3780.
(13) Peczak, P.; Luton, M. J.; *Philos. Mag. B* **1994**, *70*, 817.
(14) Bradley, R. S. *J. Phys. Chem*. **1956**, *60*, 1347.
(15) Sestak, J.; Berggren, G. J. *Thermochim. Acta* **1971**, *3*, 1.
(16) Starink M. J.; Zahra A.-M. *Thermochim. Acta* **1997**, *292*, 159.
(17) Darroudi, T.; Searcy, A. W. *J. Phys. Chem.* **1981**, *85*, 3971.
(18) Criado, J. M.; Gonzalez, M.; Malek, J.; Ortega, A. *Thermochim. Acta* **1995**, *254*, 121.
(19) Jacobs, P. W. M. *J. Phys. Chem.* **1997**, *101*, 10086−10093.
(20) Burnham, A. K. *J. Therm. Anal. Calorim.* **2000**, *60*, 895.
(21) Nam, J. D.; Seferis, J. C. *J. Polym. Sci. B: Polym. Phys*. **1992**, *30*, 455.
(22) Siele, V. I.; Warman, M.; Leccacorci, J.; Hutchinson, R. W.; Motto, R.; Gilbert, E. E.; Benzinger, T. M.; Coburn, M. D.; Rohwer, R. K.; Davey, R. K. *Propellants Explos.* **1981**, *6*, 67.
(23) Bershtein, V. A.; Egorov, V. M. *Differential Scanning Calorimetry of Polymers*; Ellis Harwood Limited: Chichester, 1994.
(24) Miles C. A.; Burjanadze T. V.; Bailey A. J. *J. Mol. Biol.* **1995**, *245*, 248−255.
(25) Brill T. B.; Karpowicz, R. J. *J. Phys. Chem*. **1982**, *86*, 4280.
(26) Karpowicz R. J.; Brill, T. B. *Appl. Spectrosc*. **1983**, *37*, 79.
(27) Henson, B. F.; Asay, B. W.; Sander, R. K.; Son, S. F.; Robinson, J. M.; Dickson, P. M. *Phys. Rev. Lett.* **1999**, *82*, 1213.
(28) Smilowitz, L.; Henson, B. F.; Asay, B. W.; Dickson, P. M. *J. Chem. Phys.* **2002**, *117*, 3789.
(29) Saw C. K. Kinetics of HMX and Phase Transitions: Effects of Grain Size at Elevated Temperature. In *Proceedings of the 12th International Detonation Symposium*, San Diego, CA, 2002; in press.
(30) Saw C. K.; Tarver C. M. In *Shock Compression of Condensed Matter 2003*; Furnish, M. D., Gupta, Y. M., Forbes, J. W., Eds.; AIP Press: 2004, pp 1029−1032.
(31) Zaug, J. M.; Farber, D. L.; Saw, C. K.; Weeks, B. L. *Kinetics of Solid-Phase Reactions at High Temperature*; Lawrence Livermore National Laboratory Report UCRL-ID-147389, February 11, 2003.
(32) Burnham, A. K.; Braun, R. L.; Coburn, T. T.; Sandvik, E. I.; Curry, D. J.; Schmidt, B. J.; Noble, R. A. *Energy Fuels* **1996**, *10*, 49.